INSTITUT DE FRANCE
Académie des sciences

Comptes Rendus
Mécanique

Elhadj B. Barry, Harunori N. Yoshikawa, Changwoo Kang, Antoine Meyer, Martin Meier, Olivier Crumeyrolle, Christoph Egbers and Innocent Mutabazi

Thermoelectric convection in a planar capacitor: theoretical studies and experiments in parabolic flights

Volume 351, Special Issue S2 (2023), p. 273-287

Published online: 8 February 2023

https://doi.org/10.5802/crmeca.143

Part of Special Issue: Physical Science in Microgravity within the Thematic Group Fundamental and Applied Microgravity

Guest editors: Olga Budenkova (CNRS, Université Grenoble Alpes,Grenoble INP, SIMaP, 38000 Grenoble, France), Catherine Colin (IMFT, Université de Toulouse, CNRS, INPT, UPS et GDR 2799 Micropesanteur Fondamentale et Appliquée) and Guillaume Legros (ICARE, CNRS UPR 3021, Univ. Orléans et GDR 2799 Micropesanteur Fondamentale et Appliquée)

Les Comptes Rendus. Mécanique *sont membres du Centre Mersenne pour l'édition scientifique ouverte*
www.centre-mersenne.org
e-ISSN : 1873-7234

Comptes Rendus
Mécanique
2023, Vol. 351, Special Issue S2, p. 273-287
https://doi.org/10.5802/crmeca.143

Physical Science in Microgravity within the Thematic Group Fundamental and Applied Microgravity / *Sciences physiques en microgravité au sein du GDR Micropesanteur Fondamentale et Appliquée*

Thermoelectric convection in a planar capacitor: theoretical studies and experiments in parabolic flights

Convection thermoélectrique dans un condensateur plan : études théoriques et expériences lors des vols paraboliques

Elhadj B. Barry [a], Harunori N. Yoshikawa [b], Changwoo Kang [c], Antoine Meyer [d], Martin Meier [d], Olivier Crumeyrolle [a], Christoph Egbers [d] and Innocent Mutabazi [*, a]

[a] Normandie Université, UNIHAVRE, LOMC, UMR CNRS 6294, 53, rue de Prony, 76058 Le Havre Cedex, France

[b] Université Côte d'Azur, INPHYNI, 06100 Nice Cedex, France

[c] Department of Mechanical Engineering, Jeonbuk National University, 567 Baekje-daero, Deokjin-gu, Jeonju-si, Jeollabuk-do, 54896, Republic of Korea

[d] Department of Aerodynamics and Fluid Mechanics, Brandenburg University of Technology Cottbus-Senftenberg, Siemens-Halske-Ring 15a, 03046 Cottbus, Germany

E-mails: elhadj-boubacar.barry@univ-lehavre.fr (E. B. Barry), Harunori.Yoshikawa@univ-cotedazur.fr (H. N. Yoshikawa), changwoo.kang@jbnu.ac.kr (C. Kang), meyer@b-tu.de (A. Meyer), meyer@b-tu.de (M. Meier), olivier.crumeyrolle@univ-lehavre.fr (O. Crumeyrolle), egbers@b-tu.de (C. Egbers), innocent.mutabazi@univ-lehavre.fr (I. Mutabazi)

Abstract. Thermoelectric convection in a plane capacitor is investigated in a microgravity environment and in the case of the thermal stable and unstable stratification in terrestrial conditions. Energetic analysis shows that in the thermal stable stratification, the thermoelectric convection is delayed while in the thermal unstable stratification, it is enhanced by the Archimedean buoyancy before the latter takes over the dielectrophoretic buoyancy and drives natural thermal convection. An experiment in parabolic flights shows the formation of thermoelectric convection at the end of the microgravity phase.

* Corresponding author.

Résumé. Nous avons étudié la convection thermoélectrique dans un condensateur plan placé dans un environnement de microgravité et dans des conditions terrestres avec une stratification thermique instable ou stable. L'analyse énergétique montre que dans le cas de stratification stable, la convection thermoélectrique est retardée alors que dans le cas de stratification thermique instable, elle est amplifiée par la poussée d'Archimède avant que cette dernière ne prenne le dessus et pilote la convection thermique naturelle. Une expérience réalisée lors des vols paraboliques illustre la formation de la convection thermoélectrique à la fin de la phase de microgravité.

Keywords. Thermoelectric convection, Dielectrophoretic force, Electric gravity, Zero-gravity, Convective patterns.

Mots-clés. Convection thermoélectrique, Force diélectrophorétique, Gravité électrique, Gravité zéro, Motifs de convection.

Published online: 8 February 2023

1. Introduction

The problem of heat transfer in microgravity conditions or in a low-gravity environment represents a scientific and technological issue to be addressed thoroughly with the development of long-term missions for space exploration. Heat transfer in fluids can be achieved through three well-identified mechanisms: heat conduction, thermal convection, and radiation. Among the three mechanisms, thermal convection represents the most efficient way to transfer heat from one surface to another through a given fluid. In many applications, thermal convection is forced by external mechanisms which are often cumbersome, especially in space devices where the weight and volume need to be optimized. In microgravity, natural convection cannot be achieved because of weak Archimedean buoyancy. Thus, to create natural-like convection, physicists have suggested using either electric force acting on dielectric liquids [1] or magnetic force acting on ferrofluids [2]. When an electric field acts on a dielectric liquid, it generates a dielectric force [1] which contains a conservative term and non-conservative component responsible for the vorticity generation. The last force called dielectrophoretic force generates thermoelectric convection when coupled with a temperature gradient in the liquid [3]. In the case of a magnetic field acting on a ferrofluid with a temperature gradient, a similar but thermomagnetic force is responsible for thermomagnetic convection generation [4].

Many studies have focused on the thermoelectric convection in spherical and cylindrical cavities because of the intense values of the dielectrophoretic force due to the inhomogeneity of the electric field induced by the curvature and because of its potential applications in the modeling of convection generation in planets [5–10]. Despite their simplicity, thermoelectric convection in rectangular cavities has been less investigated [11–13] in particular because the electric gravity is less effective than in curved configurations. However, because of the development of microfluidic systems, it is possible to achieve strong electric fields between two parallel plates distant of few microns for small values of the applied electric tension [14].

The present study addresses the linear stability analysis of the thermoelectric convection in a rectangular cavity in microgravity and thermally stable or unstable stratification. The choice of stable or unstable thermal stratification is motivated by the applications where it is either needed to evacuate heat or to enhance heat transfer between two surfaces separated by a dielectric liquid in Earth conditions. Both numerical simulations around the threshold and experiments under microgravity conditions have been performed to characterize flow patterns. The paper is organized as follows. The next section presents the physical system under investigation. Section 3 gives the base state and linearized equations near the base state. In Section 4, the linear stability results and the thermo-convective patterns are presented and discussed. Section 5

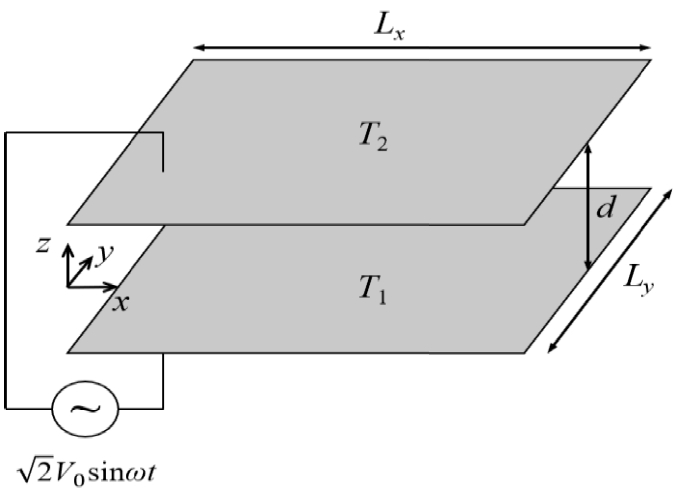

Figure 1. Dielectric liquid confined between two horizontal plates with dimensions (L_x, L_y) differentially heated $(T_1 \neq T_2)$ and with a fast alternating electric tension of frequency $f = \omega/2\pi$.

is dedicated to the experimental results. The last section contains discussions and concluding remarks.

2. Problem formulation

We consider a dielectric liquid confined between two horizontal plates differentially heated and subject to an alternating electric tension $V(t) = \sqrt{2}\,V_0 \sin\omega t$ as shown in Figure 1. The fluid is characterized by the density ρ, the kinematic viscosity ν, the thermal diffusivity κ and the electric permittivity ϵ.

The electric field $\vec{E}$ induces in the fluid a volume force called electrohydrodynamic force density which is given by [1]

$$\vec{f}_{\mathrm{EHD}} = \rho_e \vec{E} + \vec{\nabla}\left[\frac{\rho}{2}\left(\frac{\partial \epsilon}{\partial \rho}\right)_T \vec{E}^2\right] - \frac{\vec{E}^2}{2}\vec{\nabla}\epsilon \tag{1}$$

where ρ_e is the density of electric charges. The first term in (1) is the Coulomb force density, the second term is the electrostriction force density and the last term in (1) is the dielectrophoretic force $\vec{f}_{\mathrm{DEP}}$. If the frequency of the electric tension is chosen much larger than all the inverses of characteristic times of the dielectric fluid (charge relaxation, thermal diffusion and viscous times) i.e. $(\tau_e^{-1}, \tau_\kappa^{-1}, \tau_\nu^{-1}) = (\sigma_{el}/\epsilon, \kappa/d^2, \kappa/d^2) \ll f$, then it is possible to neglect the charge accumulation in the fluid so that the Coulomb force is negligible. Moreover, it is then possible to use the time-averaged electric potential instead of the alternating one. In addition to the physical phenomena described above, the displacement due to the polarization produces internal heating in the fluid when the frequency of the applied electric field is too large [15]. So, to highlight the effect of the dielectrophoretic force, we assume that the dielectric heating, arising from the dielectric loss, is negligible.

2.1. *Dielectrophoretic buoyancy and electric gravity*

We assume the electrohydrodynamic Boussinesq approximation i.e. $\rho(\theta) = \rho_0(1 - \alpha\theta)$; $\epsilon(\theta) = \epsilon_{\mathrm{ref}}(1 - e\theta)$ where $\theta = T - T_{\mathrm{ref}}$ is the deviation from the reference temperature, $\rho_0 = \rho(\theta =$

0), α is the thermal expansion coefficient and e is the thermal coefficient of the permittivity. The reference temperature is the average temperature of the two plates i.e. $T_{\text{ref}} = (T_1 + T_2)/2$. The density of the dielectrophoretic force in (1) becomes

$$\vec{f}_{\text{DEP}} = \vec{\nabla}\left[\left(\frac{\rho}{2}\left(\frac{\partial \epsilon}{\partial \rho}\right)_T + \epsilon - \epsilon_0 + \epsilon_{\text{ref}}\right)\vec{E}^2\right] - \alpha\rho_0\theta\vec{g}_e \tag{2}$$

ϵ_0 is the vacuum permittivity. The first term is a conservative force density, which represents the gradient of the electric contribution to the fluid pressure, the second term is a non-conservative force density and it is the source of the vorticity. It is written in analogy with the Archimedean buoyancy ($-\alpha\rho_0\theta\vec{g}$) and it will be called *dielectrophoretic buoyancy* with $\vec{g}_e = -\vec{\nabla}\Psi$ defined as the electric gravity where $\Psi = -e\epsilon_{\text{ref}}\vec{E}^2/2\rho_0\alpha$ is the analog of the gravitational potential and it is proportional to the electrostatic energy density stored in the capacitor. Values of properties of some dielectric liquids used in microgravity experiments are given in [13].

2.2. *Dimensionless governing equations*

We chose the characteristic scales d for lengths, ν/d for velocities, viscous diffusion time d^2/ν for time, $\Delta T = T_1 - T_2$ for temperature and V_0 for potential. The governing equations are the mass conservation equation, the momentum equation, the energy equation, and the Gauss law (charge conservation) which, in dimensionless form, read

$$\vec{\nabla}\cdot\vec{u} = 0, \tag{3a}$$

$$\frac{\partial \vec{u}}{\partial t} + (\vec{u}\cdot\vec{\nabla})\vec{u} = -\vec{\nabla}\pi + \Delta\vec{u} + Pr^{-1}\theta(Ra\vec{e}_z - L\vec{\hat{g}}_e), \tag{3b}$$

$$Pr\left[\frac{\partial\theta}{\partial t} + (\vec{u}\cdot\vec{\nabla})\theta\right] = \Delta\theta, \tag{3c}$$

$$\vec{\nabla}\cdot[(1-\gamma_e\theta)\vec{\nabla}\phi] = 0, \tag{3d}$$

where $\vec{u}$ represents the velocity field, $\gamma_e = e\Delta T$ is the thermoelectric coupling parameter, $\vec{\hat{g}}_e = \vec{g}_e/g_e$ and ϕ is the electrostatic potential i.e. $\vec{E} = -\vec{\nabla}\phi$. We have introduced the following dimensionless control parameters: the Prandtl number $Pr = \nu/\kappa$, the Rayleigh number $Ra = \alpha\Delta T g d^3/\nu\kappa$, the electric Rayleigh number $L = \alpha\Delta T\overline{g}_e d^3/\nu\kappa$ where the electric gravity $\overline{g}_e$ is computed at the central position $z = 0$ of the cavity. The quantity π represents the dimensionless hydraulic charge (Bernoulli function) [13].

The boundary conditions at the plates of the capacitor are given by:

$$u = v = w = 0, \quad \theta = \tfrac{1}{2}, \quad \phi = 1 \text{ at } z = -\tfrac{1}{2}, \tag{4a}$$

$$u = v = w = 0, \quad \theta = -\tfrac{1}{2}, \quad \phi = 0 \text{ at } z = +\tfrac{1}{2}. \tag{4b}$$

3. Base state and linear stability theory

In this section, we assume that the system has infinite extent both in the x and y directions i.e. $L_x \to \infty, L_y \to \infty$.

3.1. *Base state*

The base state is a quiescent state ($\vec{u} = 0$). The temperature, the electric potential, and the electric field depend only on the z coordinate as follows [12, 13]:

$$\theta_b(z) = -z \tag{5a}$$

$$\phi_b(z) = \ln\left(\frac{1+\gamma_e z}{1+\frac{\gamma_e}{2}}\right)\left[\ln\left(\frac{2-\gamma_e}{2+\gamma_e}\right)\right]^{-1} \tag{5b}$$

$$E_b(z) = -\frac{\gamma_e}{(1+\gamma_e z)\ln\left(\frac{2-\gamma_e}{2+\gamma_e}\right)} \tag{5c}$$

The characteristic gravity is chosen at the center of the cavity ($z = 0$) i.e.

$$\overline{g}_e = \frac{\varepsilon_{\text{ref}} e V_0^2 \gamma_e^3}{\alpha \rho_0 d^3}\left[\ln\left(\frac{1-\gamma_e/2}{1+\gamma_e/2}\right)\right]^{-2}$$

and the dimensionless electric gravity profile of the base state is given by

$$\hat{g}_{eb}(z) = -\left(1+\gamma_e z\right)^{-3} \tag{6}$$

3.2. *Linear stability analysis*

The linear stability theory consists of the superposition of infinitesimal perturbations to the base flow and then in the linearization of the resulting equations around the base state solution:

$$(u, v, w, \pi, \theta, \phi) = (0, 0, 0, \pi_b, \theta_b, \phi_b) + (u', v', w', \pi', \theta', \phi'), \tag{7}$$

where the prime denotes the perturbations. The horizontal cavity is assumed infinite in the horizontal directions so that the perturbations can be expanded into normal modes:

$$\begin{bmatrix} u'(x,y,z,t) \\ v'(x,y,z,t) \\ w'(x,y,z,t) \\ \pi'(x,y,z,t) \\ \theta'(x,y,z,t) \\ \phi'(x,y,z,t) \end{bmatrix} = \begin{bmatrix} U(z) \\ V(z) \\ W(z) \\ \Pi(z) \\ \Theta(z) \\ \Phi(z) \end{bmatrix} \exp[st + \mathrm{i}(k_x x + k_y y)] + \text{c.c.} \tag{8}$$

where $s = \sigma + \mathrm{i}\omega$ is the complex growth rate of the perturbations with σ the real growth rate and ω the frequency, k_x and k_y are the wavenumbers along the horizontal x and y directions respectively; c.c. represents the complex conjugate term. The perturbations in the temperature and the electric field induce a perturbation of the electric gravity $\vec{g}_e'$ (i.e. $\vec{g}_e = \vec{g}_{e_b} + \vec{g}_e'$) which can also be expanded into normal modes:

$$\vec{g}_e' = (G_{e_x}\vec{e}_x + G_{e_y}\vec{e}_y + G_{e_z}\vec{e}_z)\exp[st + \mathrm{i}(k_x x + k_y y)]. \tag{9}$$

The amplitudes of the normal mode of the electric gravity perturbation can be written as follows

$$\left.\begin{aligned} G_{ex} &= f(\gamma_e)(\mathrm{i}k_x D\phi_b D\Phi) \\ G_{e_y} &= f(\gamma_e)(\mathrm{i}k_y D\phi_b D\Phi) \\ G_{e_z} &= f(\gamma_e) D(D\phi_b D\Phi) \end{aligned}\right\} \tag{10}$$

where $f(\gamma_e) \equiv (1/\gamma_e^3)[\ln((1-\gamma_e/2)/(1+\gamma_e/2))]^2$. The continuity equation for the perturbation $\vec{u}'$ suggests introducing the quantity $l\hat{U} = k_x U + k_y V$ in order to reduce the problem to a 2-dimensional one.

Substitution into the linearized equation leads to

$$\left.\begin{aligned} \mathrm{i}l\hat{U} + DW &= 0 \\ sl\hat{U} &= -\mathrm{i}k^2\Pi + (D^2-k^2)l\hat{U} - \frac{L}{Pr}\theta_b(k_x G_{e_x} + k_y G_{e_y}) \\ sW &= -D\Pi + (D^2-k^2)W + \frac{1}{Pr}(Ra - L\hat{g}_{eb_0})\Theta - \frac{L}{Pr}\theta_b G_{e_z} \\ s\Theta &= W + \frac{1}{Pr}(D^2-k^2)\Theta \\ [(1+\gamma_e z)(D^2-k^2) + \gamma_e D]\Phi - \gamma_e(D^2\phi_b + D\phi_b D)\Theta &= 0 \end{aligned}\right\} \tag{11}$$

The elimination of the pressure and the use of relations (10) leads to the following system of coupled equations for W, Θ, and Φ:

$$(D^2-k^2-s)(D^2-k^2)W - \frac{k^2}{Pr}(Ra - L\hat{g}_{eb})\Theta + \frac{L}{Pr}f(\gamma_e)k^2 D\phi_b D\Phi = 0, \tag{12a}$$

$$(D^2-k^2-s\,Pr)\Theta = -Pr\,W, \tag{12b}$$

$$[(1+\gamma_e z)(D^2-k^2) + \gamma_e D]\Phi - \gamma_e(D^2\phi_b + D\phi_b D)\Theta = 0, \tag{12c}$$

where $k^2 = k_x^2 + k_y^2$. The axial velocity component can be eliminated to get a coupled system of equations for the perturbations of the temperature Θ and of the electric potential Φ:

$$[(D^2-k^2-s)(D^2-k^2-s\,Pr)(D^2-k^2) + k^2(Ra - L\hat{g}_{eb})]\Theta - Lf(\gamma_e)k^2 D\phi_b D\Phi = 0, \tag{13a}$$

$$[(1+\gamma_e z)(D^2-k^2) + \gamma_e D]\Phi - \gamma_e D(D\phi_b\Theta) = 0. \tag{13b}$$

The system (13) contains the Rayleigh–Bénard convection as a limit case when $L = 0$ and $\Phi = 0$ [16]. From the system of Equations (13), one deduces immediately that stationary modes ($s = 0$) are independent of Pr as in the Rayleigh–Bénard convection [16]. This was confirmed by the works of Roberts [3] and Yoshikawa *et al.* [12]. From the system of Equations (13), we retrieve the equations solved by Roberts [3] and Stiles [11] if we neglect the perturbative gravity terms i.e. the last terms in Equations (13a), (13b). The system of Equations (12) or (13) shows that the perturbations wavenumber intervenes through its modulus.

The amplitudes of the perturbations described by the system of Equations (11) satisfy the eigenvalue problem

$$\overline{\overline{\mathrm{L}}}\vec{\Psi} = \mathrm{s}\overline{\overline{\mathrm{M}}}\vec{\Psi}, \tag{14}$$

where the vector $\vec{\Psi}$ represents the perturbation eigenvector,

$$\vec{\Psi}(z) = \left[\hat{U}\ W\ \Pi\ \Theta\ \Phi\right]^t \tag{15}$$

where the expressions of the operators $\overline{\overline{\mathrm{L}}}$ and $\overline{\overline{\mathrm{M}}}$ are obtained from the system (11).

The boundary conditions impose that perturbations vanish at the hot and the cold parallel plates:

$$\vec{\Psi}(z = \pm 1/2) = 0. \tag{16}$$

The eigenvalue problem allows for the determination of the complex growth rate (s) of the perturbations as a function of the wavenumber $\vec{k}$ and of the control parameters (Ra, L, Pr, γ_e). Thus, solving this eigenvalue problem is equivalent to finding the following characteristic equation:

$$F(Ra, L, Pr, \gamma_e, \sigma, \omega, k) = 0. \tag{17}$$

This problem is then solved by the spectral collocation method. All unknown functions are expanded into the Chebyshev polynomial series and equations are discretized at the Chebyshev–Gauss–Lobatto collocation points [7]. The highest order of the Chebyshev polynomials series is fixed to $N = 32$ to ensure the convergence of solutions. The discretized problem is then solved by the QZ-decomposition method.

Table 1. Critical parameters (L_c, k_c) for $Pr = 11.03$ and given values of Ra.

Ra	-1000	-500	0	500	1000
L_c	3370.08	2749.87	2128.70	1506.58	883.51
k_c	3.294	3.260	3.227	3.192	3.160

3.3. *Direct numerical simulation*

The system of Equations (3) together with the boundary conditions (4) have also been solved using direct numerical simulations (DNS) based on the finite volume method [17]. Periodic boundary conditions have been imposed in the horizontal plane:

$$\begin{aligned}\vec{u}(x,y,z) &= \vec{u}(x \pm L_x, y \pm L_y, z)\\ \theta(x,y,z) &= \theta(x \pm L_x, y \pm L_y, z)\\ \phi(x,y,z) &= \phi(x \pm L_x, y \pm L_y, z)\end{aligned}$$

The period of the computation box ($L_x = L_y = 10$) has been chosen in order to ensure the presence of sufficient enough convective structures. A regular mesh has been fixed to 256 points in the x and y directions while in the z-direction, the mesh size was adapted near the wall with $\Delta z = 0.005$. The flow structures were visualized using the plots of the iso-surfaces of the quantity $Q = -(1/2)\mathrm{tr}\left(\overline{\overline{S}}^2 + \overline{\overline{\Omega}}^2\right)$ where $\overline{\overline{S}}$ and $\overline{\overline{\Omega}}$ represent the symmetric and the antisymmetric parts of the velocity-gradient tensor $\vec{\nabla}\vec{u}$ respectively [9, 10].

4. Results

4.1. *Critical parameters*

Ignoring the perturbative gravity terms in (11), Roberts [3] has proved the validity of the exchange of stability which claims that the marginal states are stationary ($\omega = 0$). Keeping the perturbative gravity terms, we searched for the marginal stability curves which correspond to $\sigma = 0$ and we found that the marginal states remain stationary. The minimum point of the neutral curves ($\sigma = 0$) gives the critical stability point which characterizes the onset of the thermoelectric instability in the fluid between the two parallel plates.

In their studies, Yoshikawa *et al.* [12] have shown that the threshold of thermoelectric convection in a rectangular cavity is insensitive to the values γ_e of when $\gamma_e < 0.1$. In the problem under study $\gamma_e \ll 1$. We have determined the curves of marginal stability states in the (k, L) plane (Figure 2) for various fixed values of Pr and of $Ra \in \{-12000, 1700\}$. The critical modes are stationary and the threshold L_c is insensitive to the values of Pr. We fixed $Ra \in [-12000; 0[$ which corresponds to a thermally stable stratification, $Ra \in]0; 1700]$ to an unstable thermal stratification and $Ra = 0$ which corresponds to the zero-gravity environment. The thermal stable stratification delays the onset of thermoelectric convection; while the thermal unstable stratification accelerates the thermoelectric convection, i.e. $L_c(0 < Ra < Ra_c) < L_c(Ra = 0) < L_c(Ra < 0)$. Values of critical parameters are presented in Table 1 for few values of Ra.

We also present, in Figure 3 the eigenfunctions of the critical electric mode plotted in both vertical planes (x–z) and (y–z) under microgravity conditions ($Ra = 0$) for $Pr = 11.03$. The thermoelectric convection patterns are inclined in the horizontal (x–y) plane with two wavenumbers $k_x \neq k_y \neq 0$.

The variations of the critical parameters (L_c, k_c) with Ra are shown in Figure 4 and we confirm the results [3, 12] that the critical electric mode is not sensitive to the Pr regardless of heating

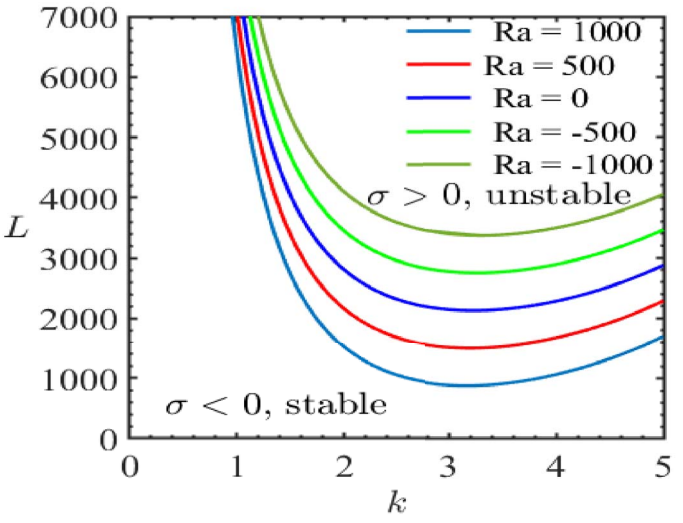

Figure 2. Marginal stability curves for $Pr = 11.03$ and $Ra \in \{-1000, -500, 0, 500, 1000\}$.

direction ($Ra < 0$ or $0 < Ra < 1708$). These variations can be approximated by linear relationships in the range of computed values of $Ra \in [-1.2 \times 10^4, 1.7 \times 10^3]$:

$$L_c = L_c^0 - C\,Ra, \quad \text{with } C = L_c^0/Ra_c^0; \quad k_c = 3.223 - 8 \times 10^{-5} Ra \tag{18}$$

here $L_c^0 = 2128.6$ is the critical electric Rayleigh number under microgravity conditions ($Ra = 0$) and $Ra_c^0 = 1708$ is the critical Rayleigh number in the classical Rayleigh–Bénard convection, so that with $C = L_c^0/Ra_c^0 = 1.247$. We recover the relationship (one obtained analytically by Stiles [11] who found $C = 1.246$ and $L_c^0 = 2128.695$. The threshold of thermoelectric convection in a thermal stable stratified liquid is larger than in microgravity while that of the thermal unstable stratified liquid is lower than that in microgravity. The size of convective structures increases with *Ra*.

4.2. *Energetic analysis near the TEHD threshold*

The equation of the kinetic energy of the perturbations is obtained by taking the scalar product of the velocity perturbation $\vec{u}'$ by the momentum equation and integrating over the volume to get

$$\frac{\mathrm{d}K}{\mathrm{d}t} = W_{\mathrm{BEG}} + W_{\mathrm{PEG}} + W_G - D_v, \tag{19}$$

where $K = \int (1/2)|\vec{u}|^2\,\mathrm{d}V$ is the kinetic energy, $W_{\mathrm{BEG}} = -(L_c/Pr)\int \theta \vec{u}' \cdot \vec{g}_{eb}\,\mathrm{d}V$ is the power of the dielectrophoretic buoyancy, $W_{\mathrm{PEG}} = -(L_c/Pr)\int (\overline{\theta}\vec{u}') \cdot \vec{g}_e'\,\mathrm{d}V$ is the power performed by the perturbation of the dielectrophoretic buoyancy, $W_G = \int \theta \vec{u}' \cdot \vec{g}\,\mathrm{d}V$ is the power performed by the Archimedean buoyancy, and $D_v = \int d_v\,\mathrm{d}V$ is the dissipation of perturbative vorticity by viscosity with

$$d_v = Re^2 \left\{ 2\left[\left(\frac{\partial u'}{\partial x}\right)^2 + \left(\frac{\partial v'}{\partial y}\right)^2 + \left(\frac{\partial w'}{\partial z}\right)^2 \right] + \left[\left(\frac{\partial v'}{\partial x} + \frac{\partial u'}{\partial y}\right)^2 + \left(\frac{\partial w'}{\partial y} + \frac{\partial v'}{\partial z}\right)^2 + \left(\frac{\partial u'}{\partial z} + \frac{\partial w'}{\partial x}\right)^2 \right] \right\}.$$

The terms of the energy equation of a flow in a system heated from the bottom are presented in Figure 5 for $Pr = 11.03$. All terms were computed for different values of $Ra < Ra_c = 1708$. The power W_G increases when increasing *Ra*; while the contribution of the basic electric gravity W_{BEG} decreases with *Ra*. In the stable thermal stratification, the Archimedean buoyancy has a negative power and the dielectrophoretic force furnishes a large power to trigger thermoelectric convection.

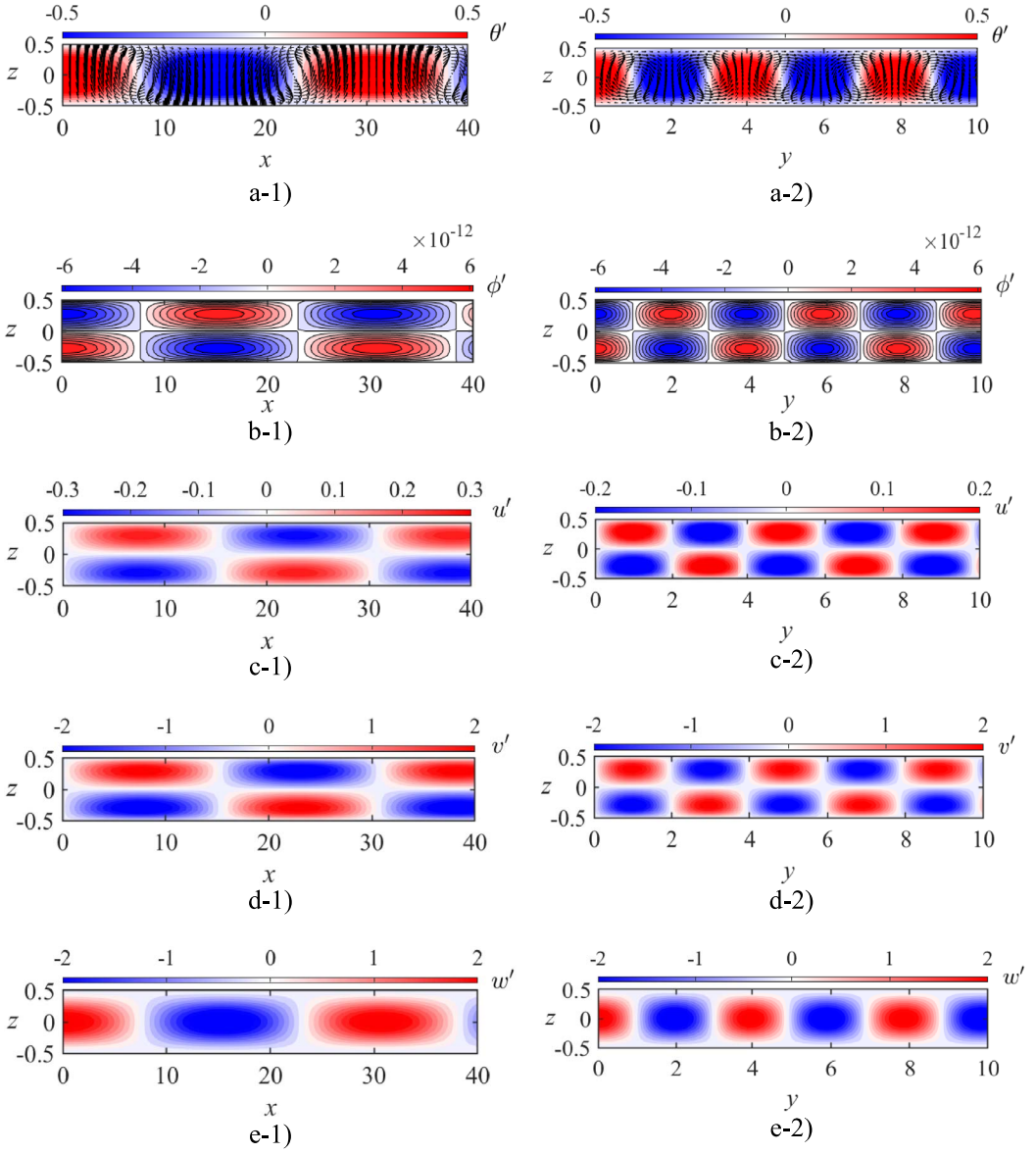

Figure 3. Eigenfunctions of the electric mode in the planes $y = 0$ and $x = 0$ for $Pr = 11.03$, $Ra = 0$, and $L_c = 2128.69$: (a) velocity fields and temperature levels, (b) electric potential ϕ', (c,d) the horizontal velocity components u' and v', and (e) the vertical velocity w'. We choose $L_x = 40$ in order to highlight the periodicity along the x-direction.

For unstable thermal stratification, Archimedean buoyancy contributes to the power of the dielectrophoretic buoyancy to induce thermoelectric convection. For $Ra^* \approx 954$, $W_G = W_{\mathrm{BEG}}$ so that for $Ra < Ra^*$, the thermoelectric convection is enhanced by the Archimedean buoyancy while for $Ra > Ra^*$, the Archimedean buoyancy furnishes the larger power in triggering thermal convection so that the dielectrophoretic force gives less power. Just below Ra_c, we obtain $W_{\mathrm{BEG}} \to 0$. So we can conclude that the thermoelectric convection occurs for $Ra < Ra^*$ while for $Ra > Ra^*$, we have Rayleigh–Bénard convection enhanced by dielectrophoretic buoyancy. The viscous

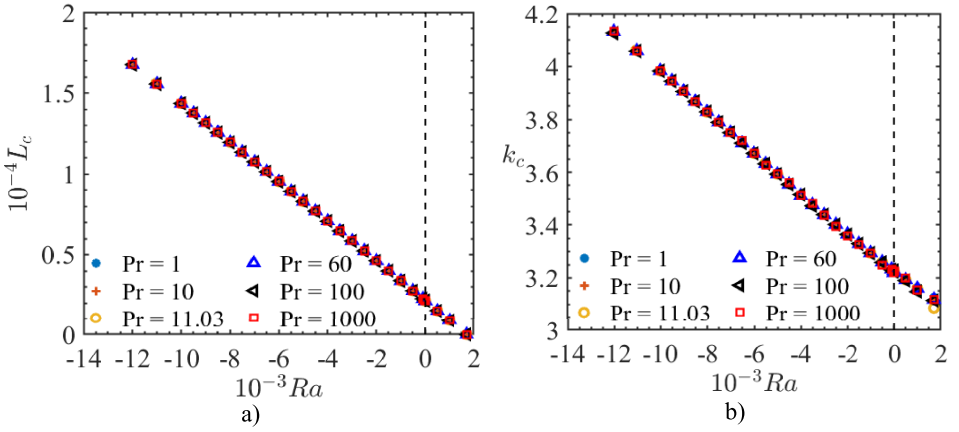

Figure 4. Variation of critical parameters against *Ra* for various values of *Pr*: (a) critical electric Rayleigh number L_c; (b) critical wavenumber k_c.

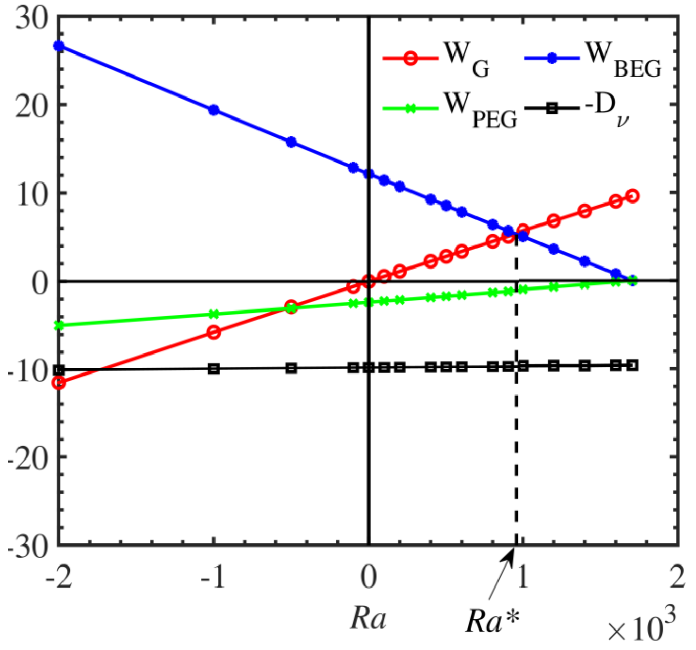

Figure 5. Different terms of the energy balance at the critical point (L_c, k_c) normalized by twice the kinetic energy plotted as a function of the Rayleigh number *Ra* (a) for *Pr* = 11.03 (Novec 7200) and $Ra \in]-2000; 1700]$.

dissipation does not change with *Ra*, while the absolute value of the power from the perturbative dielectrophoretic buoyancy decreases as *Ra* increases. This means that the power produced by the buoyancies in the fluid is tuned to balance the viscous dissipation which is independent of *Ra*.

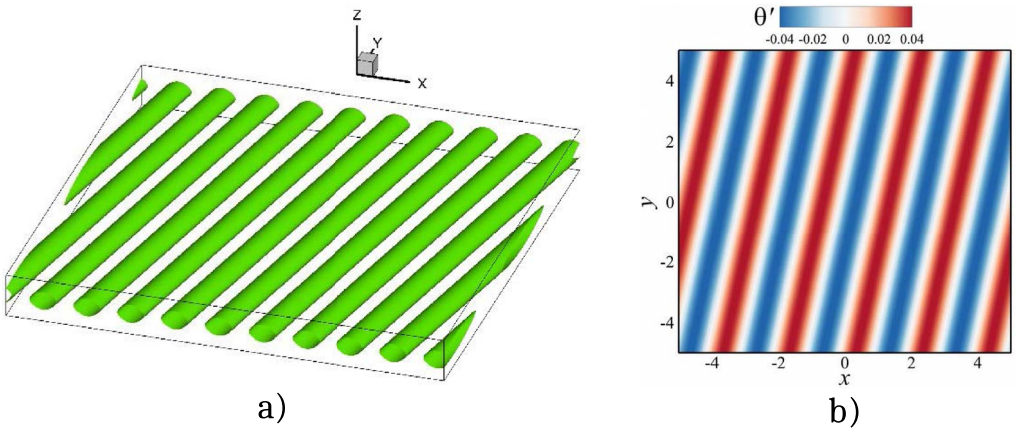

Figure 6. Flow vortical structures illustrated by (a) iso-surfaces of $Q = 4$, and (b) isotherms in the horizontal (x–y) plane for $Pr = 1$, $\gamma_e = 0.01$, $Ra = 0$ and $L = 2150$.

Table 2. Properties of the working fluid (Novec 7200 at $T = 298.15$ K).

ρ (kg·m^{-3})	α (10^{-3} K^{-1})	ν (10^{-7} m^2·s^{-1})	κ (10^{-8} m^2·s^{-1})	ϵ_r	e (10^{-3} K^{-1})	Pr	V_i (V)	V_b (kV)
1430	1.6	4.3	3.90	7.3	3.9	11.03	0.61	40

4.3. *Thermo-convective flow pattern around the threshold*

The results from DNS for $Pr = 1$ near the threshold ($\delta = (L - L_c)/L_c = 0.01$) in zero-gravity confirm the results from linear stability analysis on the inclination of convective structures in the (x–y) plane.

Figure 6a shows the iso-surfaces of Q and Figure 6b shows the isotherms of the thermo-convective patterns in the horizontal plane. Vertical cross-sections of the instantaneous fields are presented in Figure 7 and the vorticity components are illustrated in Figure 8.

5. Experimental results

We have performed experiments in a horizontal rectangular cavity of sizes ($L_x = 0.2$ m, $L_y = 0.04$ m, $d = 0.005$ m) during a parabolic flight aboard the zero-g Airbus of NOVESPACE-CNES. We fixed the value of the temperature difference ΔT between the upper and lower plates and varied the value of the applied effective electric potential V_0. The system has an accelerometer that detects the microgravity phase so that the control program can activate the high voltage at a specified instant of the parabola. The horizontally aligned cavity was heated from the top and cooled from the bottom so that the gravity phases always correspond to a thermal stable stratification. The high voltage is applied 5 s after the microgravity conditions started so the initial conditions favor the growth of thermoelectric instabilities [18].

For the given working fluid, we introduced an intrinsic electric potential $V_i = \sqrt{\rho \nu \kappa / \epsilon_{\text{ref}}}$ based on the properties of the fluid. The potential V_i is used in theoretical studies to scale the applied voltage [10]. The working dielectric liquid in the experiment was Novec 7200 ($C_4F_9OC_2H_5$), the properties of which are given in Table 2. The breakdown potential V_b of this dielectric liquid is also presented in Table 2.

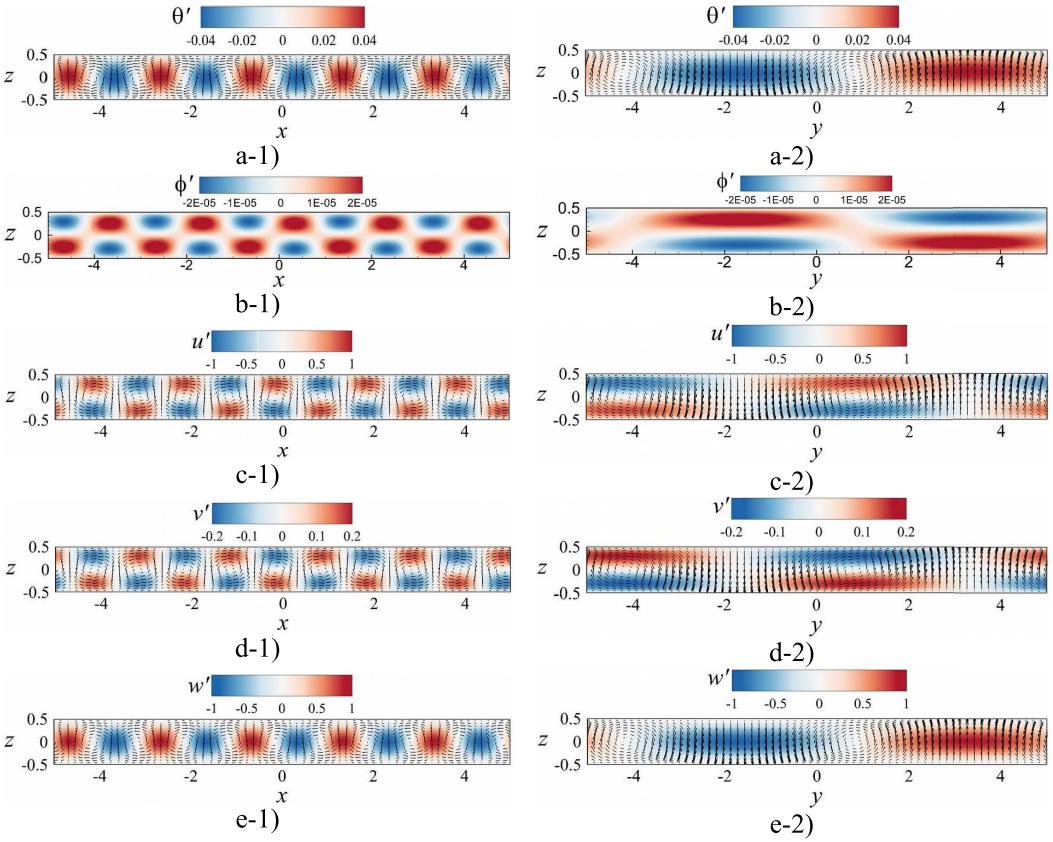

Figure 7. Instantaneous flows in the vertical planes $y = 0$ and $x = 0$ for $Ra = 0$, $Pr = 1$ and $L = 2150$. Vectors represent the velocity fields: (a) temperature distribution (color); (b) potential; (c,d) horizontal velocity component v (color); and (e) vertical velocity (color).

For flow visualization, we have used the background-oriented Schlieren technique (BOS) which is based on the variation of the refractive index of the fluid due to the density gradient [19–22]. A section of the horizontal gap is illuminated from the bottom to the top with an LED panel, to which is attached a background image composed of dots with random positions. On the other side of the gap, a camera takes pictures of the illuminated section. The density gradient can be correlated with the local optical displacement of that random pattern in the (x, y) plane compared to a reference case [20]. That reference image corresponds to the one with no applied temperature difference and no applied electric potential.

Figure 9 shows the divergence of the displacement field $(\vec{\nabla} \cdot \vec{d})$ for $\Delta T \approx 7$ K for two values of V_0. Pictures are taken at the end of the microgravity phase (0 g) so that the patterns had time to develop in the flow. The first image corresponds to the case without electric potential where the displacement field presents no particular divergence. The image is then completely correlated to the reference one, up to its homogeneous translation. However, when the potential $V_0 = 1.41$ kV is applied, and the divergence of the displacement field highlights the occurrence of alternated positive and negative areas. As the corresponding electric Rayleigh number $L = 4000$ is then nearly twice the critical value under microgravity conditions ($L_c \approx 2129$), this mode is interpreted as a result of the thermoelectric instability.

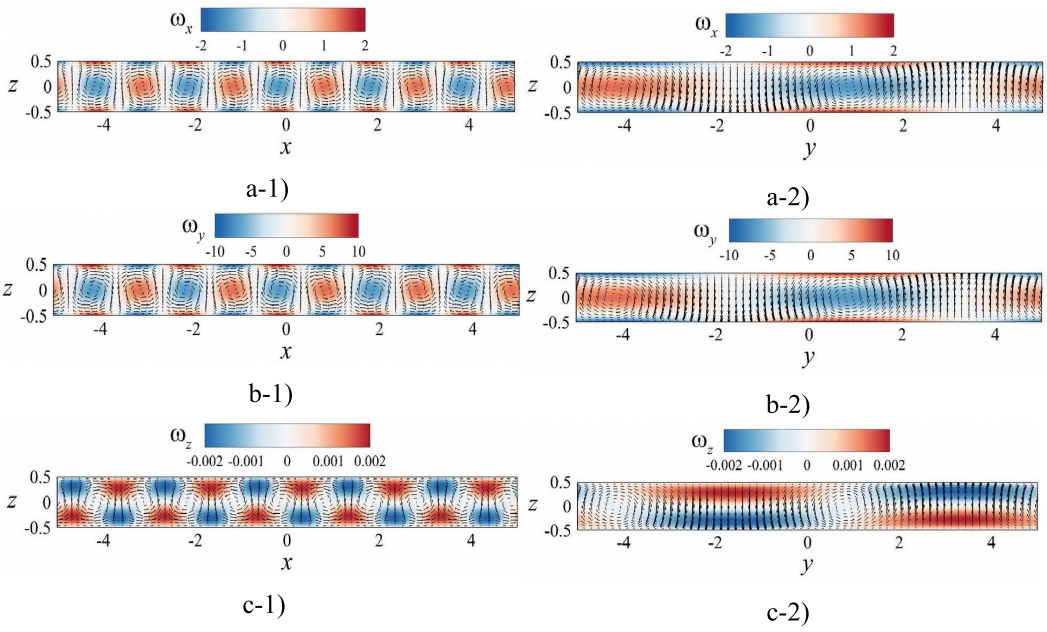

Figure 8. Vorticity components in the plane $y = 0$, and in the plane $x = 0$ for $Pr = 1$, $Ra = 0$, and $L = 2150$. Vectors represent the velocity fields: (a,b) horizontal vorticity components (color); and (c) vertical vorticity components (color).

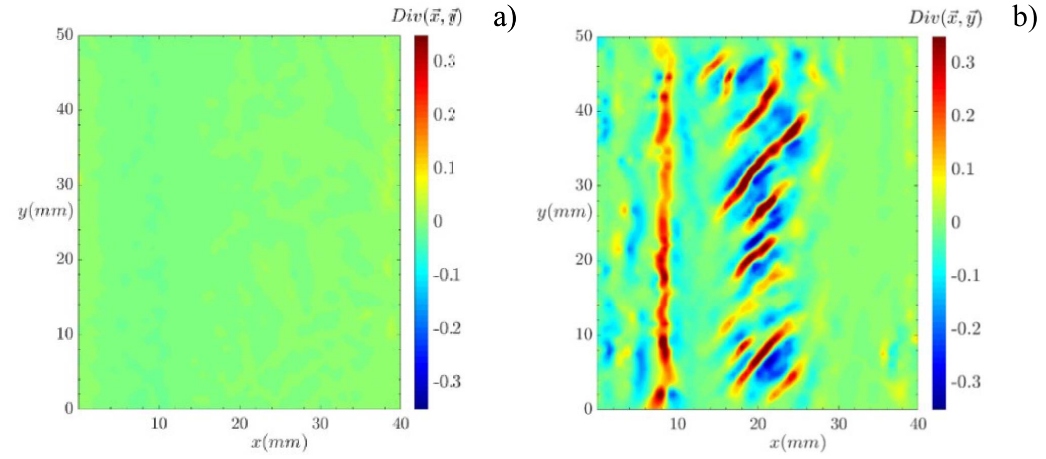

Figure 9. Patterns of the divergence of the displacement vector $(\vec{\nabla}\cdot\vec{d})$ corresponding to $\Delta T \approx 7$ K in the microgravity phase: (a) $V_0 = 0$, (b) $V_0 = 1.41$ kV.

6. Conclusion

We have performed a linear stability analysis of thermoelectric convection in a planar capacitor in microgravity and investigated the effect of the stable and unstable thermal stratification on the critical parameters. The results from zero-gravity are confirmed by the DNS. The experiment performed in parabolic flight aboard zero-g Airbus confirmed the existence of thermo-convective structures induced by the dielectric buoyancy in the microgravity phase.

Nomenclature

Symbols	Signification	Symbols	Signification
V_b	Breakdown potential	Ra	Rayleigh number
d	Cavity width	κ	Thermal diffusivity
$\vec{f}_{\mathrm{DEP}}$	Density of the dielectrophoretic force	ν	Kinematic viscosity
$\vec{E}$	Electric field	ρ	Fluid density
$\vec{g}_e$	Electric gravity	α	Thermal expansion coefficient
ϕ	Electric potential	ϵ	Permittivity
V_0	Effective electric tension	e	Thermal coefficient of the permittivity
L_x, L_y	Horizontal lengths of the cavity	γ_e	Thermoelectric coupling parameter
V_i	Intrinsic electric potential	σ_{el}	Electrical conductivity
π	Dimensionless pressure	k_x	Wavenumber along x direction
ΔT	Temperature difference	k_y	Wavenumber along y direction
T_{ref}	Reference temperature	k	Total wavenumber
θ	Temperature deviation	L	Electric Rayleigh number
s	Complex growth rate	Pr	Prandtl number

Conflicts of interest

Authors have no conflict of interest to declare.

Acknowledgments

The present work was supported partially by both the CNES (project INTEHLDI) and the DLR (Grant Nos 50WM1644 and 50WM1944), the CNRS LIA 1092 ISTROF, and the French National Research Agency (ANR) through the program "Investissements d'Avenir (Grant Nos ANR-10LABX-09-01)", LABEX EMC^3. EB benefitted from a PhD scholarship cofounded both by the CNES and the Région Normandie. CK was supported by the National Research Foundation of Korea (NRF) grant funded by the Korean Ministry of Science and ICT (MSIT) (NRF-2021K1A3A1A21039317). CK and IM acknowledge the support from the bilateral French-Korean exchange program STAR-PHC.

References

[1] L. D. Landau, E. M. Lifshitz, *Electrodynamics of Continuous Media*, Elsevier Buttherworth-Heinemann, Burlington, MA, 1984.

[2] R. E. Rosensweig, *Ferrohydrodynamics*, Cambridge University Press, Cambridge, MA, 1985.

[3] P. H. Roberts, "Electrohydrodynamic convection", *Q. J. Mech. Appl. Math.* **22** (1969), no. 2, p. 211-220.

[4] A. A. Bozhko, S. A. Suzlov, *Convection in Ferro-Nanofluids: Experiments and Theory*, Springer (eBook), 2018.

[5] J. E. Hart, G. A. Glatzmaier, J. Toomre, "Space-laboratory and numerical simulations of thermal convection in a rotating hemispherical shell with radial gravity", *J. Fluid Mech.* **173** (1986), p. 519-544.

[6] B. Futterer, A. Krebs, A.-C. Plesa, F. Zaussinger, R. Hollerbach, D. Breuer, C. Egbers, "Sheet-like and plume-like thermal flow in a spherical convection experiment performed under microgravity", *J. Fluid Mech.* **735** (2013), p. 647-683.

[7] H. N. Yoshikawa, O. Crumeyrolle, I. Mutabazi, "Dielectrophoretic force-driven thermal convection in annular geometry", *Phys. Fluids* **25** (2013), article no. 024106.

[8] V. Travnikov, O. Crumeyrolle, I. Mutabazi, "Influence of the thermo-electric coupling on the heat transfer in cylindrical annulus with a dielectric fluid under microgravity", *Acta Astronaut.* **129** (2016), p. 88-94.

[9] C. Kang, I. Mutabazi, "Dielectrophoretic buoyancy and heat transfer in a dielectric liquid contained in a cylindrical annular cavity", *J. Appl. Phys.* **125** (2019), article no. 184902.

[10] C. Kang, I. Mutabazi, "Columnar vortices induces by dielectrophoretic force in a stationary cylindrical annulus filled with a dielectric liquid", *J. Fluid Mech.* **908** (2021), article no. A26.

[11] P. J. Stiles, "Electro-thermal convection in dielectric liquids", *Chem. Phys. Lett.* **179** (1991), no. 3, p. 311-315.
[12] H. N. Yoshikawa, M. Tadie Fogaing, O. Crumeyrolle, I. Mutabazi, "Dielectrophoretic Rayleigh–Bénard convection under microgravity conditions", *Phys. Rev. E* **87** (2013), article no. 043003.
[13] M. Tadie Fogaing, H. N. Yoshikawa, O. Crumeyrolle, I. Mutabazi, "Heat transfer in the thermo-electro-hydrodynamic convection under microgravity conditions", *Eur. Phys. J. E* **37** (2014), article no. 35.
[14] Z. Liu, C. Li, B. Wang, "Flow structure and heat transfer of electro-thermo-convection in a dielectric liquid layer", *Phys. Fluids* **31** (2019), article no. 064103.
[15] H. Yoshikawa, C. Kang, I. Mutabazi, F. Zaussinger, P. Haun, C. Egbers, "Thermoelectrohydrodynamic convection in parallel plate capacitors under dielectric heating conditions", *Phys. Rev. Fluids* **5** (2020), article no. 113503.
[16] S. Chandrasekhar, *Hydrodynamic and Hydromagnetic Stability*, Dover Publications, New York, 1981.
[17] E. B. Barry, C. Kang, H. Yoshikawa, I. Mutabazi, "Transfert de chaleur par convection thermoelectrique dans des cavités rectangulaires horizontales", *Entropie* **2** (2021), no. 2, p. 1-11, ISTE Open Sciences.
[18] A. Meyer, M. Meier, M. Jongmanns, T. Seelig, C. Egbers, I. Mutabazi, "Effect of the initial conditions on the growth of thermoelectric instabilities during parabolic flights", *Microgravity Sci. Technol.* **31** (2019), p. 715-721.
[19] K. Hayasaka, Y. Tagawa, T. Liu, M. Kameda, "Optical-flow-based background-oriented Schlieren technique for measuring a laser-induced underwater shock wave", *Exp. Fluids* **57** (2016), article no. 179.
[20] G. Meier, "Computerized background-oriented Schlieren", *Exp. Fluids* **33** (2002), p. 181-187.
[21] L. Venkatakrishnan, G. E. A. Meier, "Density measurements using the background oriented Schlieren technique", *Exp. Fluids* **37** (2004), p. 237-247.
[22] M. Raffel, "Background-oriented Schlieren (BOS) techniques", *Exp. Fluids* **56** (2015), article no. 60.